DOI:
10.1016/j.media.2017.08.001

Document Version
Peer reviewed version

Citation for published version (APA):
Toth, D., Panayiotou, M., Brost, A., Behar, J. M., Rinaldi, C. A., Rhode, K. S., & Mountney, P. (2017). 3D/2D Registration with Superabundant Vessel Reconstruction for Cardiac Resynchronization Therapy. *Medical Image Analysis*, *42*, 160-172. https://doi.org/10.1016/j.media.2017.08.001

Accepted Manuscript

3D/2D Registration with Superabundant Vessel Reconstruction for Cardiac Resynchronization Therapy

Daniel Toth, Maria Panayiotou, Alexander Brost, Jonathan M. Behar, Christopher A. Rinaldi, Kawal S. Rhode, Peter Mountney

PII: S1361-8415(17)30125-1
DOI: 10.1016/j.media.2017.08.001
Reference: MEDIMA 1286

To appear in: *Medical Image Analysis*

Received date: 14 December 2016
Revised date: 31 July 2017
Accepted date: 1 August 2017

Highlights

- 3D/2D registration using adjacent anatomical structures is proposed.
- Superabundant 3D vessel reconstruction is performed without point correspondences.
- A globally optimal registration method is extended with dynamic outlier rejection.
- Novel evaluation framework using previously implanted artificial valves is proposed.

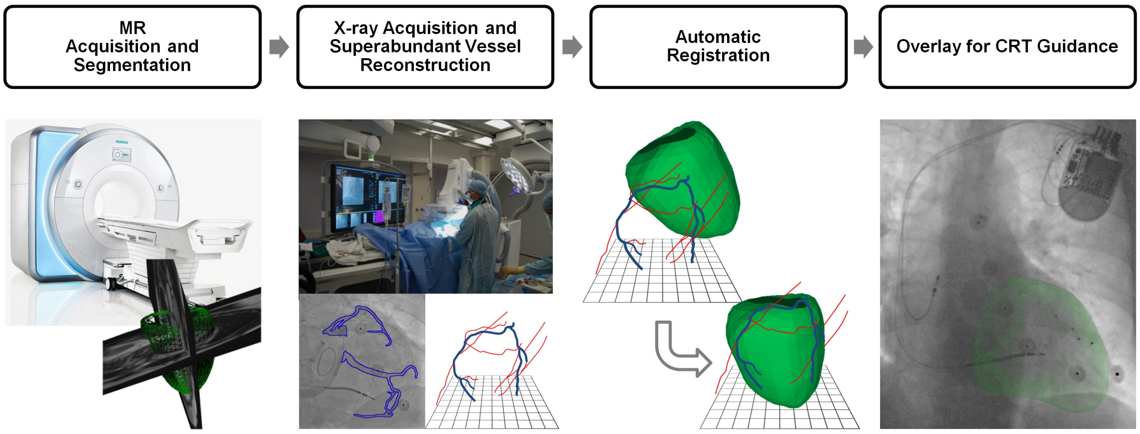
MR
Acquisition and
Segmentation
X-ray Acquisition and
Superabundant Vessel
Reconstruction
Automatic
Registration
Overlay for CRT Guidance

3D/2D Registration with Superabundant Vessel Reconstruction for Cardiac Resynchronization Therapy

Daniel Toth[a,b,*], Maria Panayiotou[b], Alexander Brost[c], Jonathan M. Behar[b,d], Christopher A. Rinaldi[b,d], Kawal S. Rhode[b,1], Peter Mountney[e,1]

[a]*Siemens Healthineers, UK*
[b]*Division of Imaging Sciences and Biomedical Engineering, King's College London, UK*
[c]*Siemens Healthineers, Germany*
[d]*Department of Cardiology, Guy's and St. Thomas' Hospitals NHS Foundation Trust, UK*
[e]*Medical Imaging Technologies, Siemens Healthineers, Princeton, NJ, USA*

Abstract

A key component of image guided interventions is the registration of preoperative and intra-operative images. Classical registration approaches rely on cross-modality information; however, in modalities such as MRI and X-ray there may not be sufficient cross-modality information. This paper proposes a fundamentally different registration approach which uses adjacent anatomical structures with superabundant vessel reconstruction and dynamic outlier rejection. In the targeted clinical scenario of cardiac resynchronization therapy (CRT) delivery, preoperative, non contrast-enhanced, MRI is registered to intraoperative, contrasted X-ray fluoroscopy. The adjacent anatomical structures are the left ventricle (LV) from MRI and the coronary veins reconstructed from two contrast-enhanced X-ray images. The novel concept of superabundant vessel reconstruction is introduced to bypass the standard reconstruction problem of establishing one-to-one correspondences. Furthermore, a new dynamic outlier rejection method is proposed, to enable globally optimal point set registration. The proposed approach has been qualitatively and quantitatively evaluated on phantom, clinical CT angiography with ground truth and clinical CRT data. A novel evaluation method is proposed for clinical CRT data based on previously

*Corresponding author
Email address: `daniel.toth@kcl.ac.uk` (Daniel Toth)
[1]Joint senior authors

implanted artificial aortic and mitral valves. The registration accuracy in 3D was 2.94 mm for the aortic and 3.86 mm for the mitral valve. The results are below the required accuracy identified by clinical partners to be the half-segment size (16.35 mm) of a standard American Heart Association (AHA) 16 segment model of the LV.

Keywords: 3D/2D Registration, Cardiac Registration, Image Guided Interventions, Cardiac Resynchronization Therapy

---

1. Introduction

Patients with advanced drug-refractory heart failure can be safely treated with Cardiac Resynchronization Therapy (CRT). However, 30 to 40 % of patients do not respond to therapy [1]. In this procedure, a CRT device is implanted using fluoroscopic image guidance. The device has 3 leads which are placed in the right atrium, right ventricle and through the coronary sinus (CS) on the surface of the left ventricle (LV). Suboptimal placement of the lead on the LV has been identified as a leading cause of non-response. Unfortunately, improving the placement of this lead is extremely challenging for clinicians.

It has been shown that placing the LV lead away from scar tissue and in the latest point of mechanical activation can improve the response rate [2]. This information cannot be directly obtained from fluoroscopic images and requires an additional imaging modality, such as preoperative magnetic resonance imaging (MRI). Registering preoperative MRI with intraoperative fluoroscopic images enables clinicians to visualize scar and mechanical activation in real time fluoroscopic overlay, guiding the placement of the LV lead to improve response rates.

Registering non contrast-enhanced MRI to fluoroscopy remains an open research problem. The main challenge is the lack of shared information between the modalities. In the case of cardiac MRI, the images show high soft tissue contrast to visualize the heart, but bony structures, such as the spine, are not easily seen. In fluoroscopic images however, bony structures and instruments are well visible, but there is a lack of contrast for soft tissue. The only way to visualize soft tissue anatomy is to inject contrast agent. In CRT this is used to visualize the CS. The registration problem is further complicated by different fields of view, the low resolution of MRI and cardiac and respiratory motions.

Current approaches for registering MRI to fluoroscopy can be categorized as manual, fiducial-, tool- or anatomical landmark-based methods. Manual registration is technically simple, but practically challenging due to the nature of registering a 3D image to a 2D image without strong landmarks. The process is time consuming and highly user dependent. Fiducial markers which are visible in both modalities can be placed on the patient for matching [3], or on the components of the imaging system for tracking [4]. This solves the registration problem, but introduces workflow challenges and requires the MRI to be acquired directly before the procedure which is not feasible for most hospitals. Tool based methods [5, 6] use prior knowledge that a guidewire or catheter will be in the vessels (e.g. CS) during the procedure. By detecting the tool in the fluoroscopic images, the 3D position of the vessel can be inferred and registered to the centerline of the same vessels segmented from the preoperative MRI. An additional high resolution whole heart MRI is required which is not always feasible to acquire with heart failure patients. The accuracy of this approach can be affected by the tool deforming the vessel and the image guidance overlay cannot be used until the tools have been placed inside the vessels, making a less attractive clinical workflow. A fundamentally different tool-based method simulates the alignment of a catheter in the CS based on a preoperative 3D acquisition and registers the simulated catheter to a real device during the intervention [7]. A notable approach for CRT, fuses the CS extracted from fluoroscopy with single-photon emission computed tomography (SPECT) [8, 9] for 3D visualization. A 3D model of the vessels is generated from contrasted fluoroscopy and warped to the surface of meshes segmented from SPECT images. This approach is not used for image overlay and relies on corresponding landmarks which is challenging in low resolution of SPECT images. Our goal is to develop an image guided navigation system that 1) has a workflow suitable to all hospitals, does not require fiducials, 2) does not require lengthy additional MR acquisitions and 3) can be used early in the procedure before tools are inserted into vessels.

This paper presents a method for registering adjacent anatomical structures, similarly to [10], but for cardiac registration, and introduces the concepts of superabundant vessel reconstruction and dynamic outlier rejection. It extends preliminary work [11] on registering adjacent anatomy, the LV (from non contrast-enhanced MRI) to the coronary veins (from contrast-enhanced X-ray fluoroscopy), for CRT procedures. This approach is highly suitable for X-ray/MRI registration as is does not use cross-modality information; however, it requires the vessel system to be reconstructed from two X-ray images and the relatively sparse vessel system to be registered to the surface of the LV.

Reconstructing the vessel system is challenging in CRT where contrast washes quickly out of the veins and the two X-ray images are acquired sequentially with separate and potentially inconsistent contrast injections. The problem is exacerbated by varying quality of occlusion and missing vessels. For reconstructing coronary arteries, approaches that match bifurcations have been proposed [12], but for CRT, coronary vein reconstruction techniques require manual vessel matching [8, 9]. This paper proposes superabundant vessel reconstruction which explicitly removes the need to perform vessel matching. The reconstructed vessel model is guaranteed to contain the true vessel structure and additional outliers.

The reconstructed coronary vein model is sparse relative to the LV surface. Registering these two structures is a partial surface registration problem which is well known to get stuck in local minima, especially when the data contains outliers. To overcome this challenge, a novel dynamic outlier rejection method is proposed. Outliers are estimated in the vessel reconstruction phase and combined with a globally optimal registration framework to prevent the registration from becoming stuck in local minima.

The accuracy of the proposed system is evaluated on phantom and *in vivo* data. A novel validation framework is proposed that exploits artificial valves implanted in the patients. The clinical application is demonstrated on patient data and evaluated by surveying a team of clinical experts.

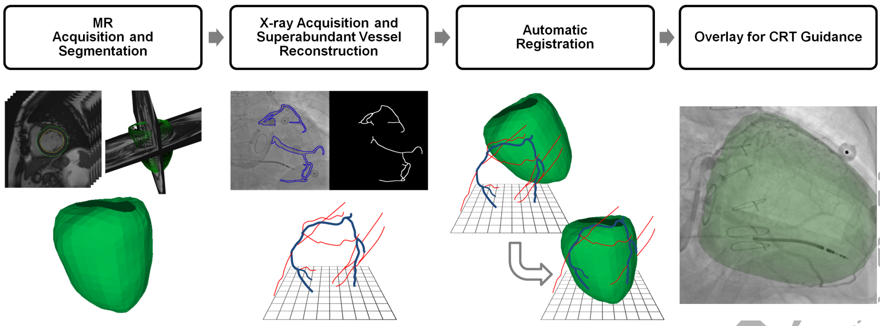

Figure 1: Workflow steps of proposed registration framework.

2. Methods

2.1. Overview

Classical registration approaches for medical images from different modalities rely on matching anatomical structures or landmarks that are present and visible in both images. These are known as cross-modality landmarks. MR and X-ray fluoroscopy images are intrinsically different and cross-modality landmarks are often not easily identifiable or even present. This work proposes a novel approach that uses anatomical structures that are adjacent to each other. In CRT the two adjacent structures are: 1) the LV epicardium (from MRI) and 2) the venous anatomy on the LV, the CS and the branching coronary veins (from fluoroscopy).

The main steps of the proposed method are depicted in Figure 1. Pre-operative MRI images are automatically segmented and a 3D model of the LV epicardium is generated. Intraoperatively, the coronary veins are extracted from two frame-matched fluoroscopic images and a superabundant 3D vessel model is automatically reconstructed. Finally, the 3D vessel model is registered to the LV epicardial mesh with a globally optimal iterative closest points (Go-ICP) method [13, 14] where outliers are modelled using information derived from the superabundant vessel reconstruction step.

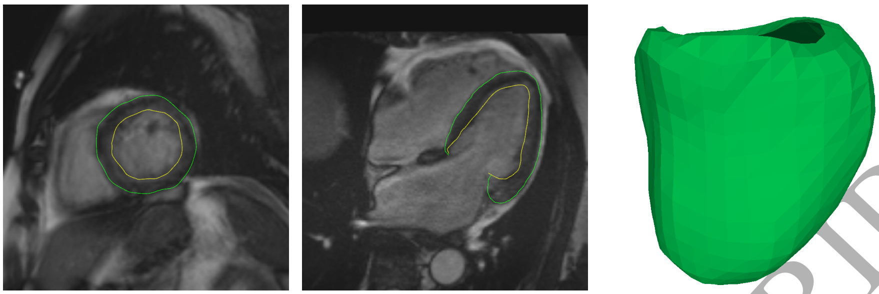

(a) (b) (c)

Figure 2: MR image segmentation. (a) Segmented short axis slice. (b) Segmented long axis slice. (c) Reconstructed 3D epicardial shell.

2.2. LV epicardial model

The epicardial mesh is generated from the automatically segmented MRI. The SA and LA MR images are segmented with a combination of a machine learning based landmark detection and grey level analysis [15]. The contours of the epicardium are extracted using a minimum path algorithm based on histogram analysis in every slice, see Figure 2 (a,b). The resulting contours are propagated through all phases by distortion fields and are used to generate a 3D mesh model of the epicardium for each heart phase over the cardiac cycle, see Figure 2 (c). The end diastolic mesh is selected for registration.

2.3. Vascular 3D model reconstruction

2.3.1. Fluroscopic frame gating

In the current CRT workflow a monoplane fluoroscopic system is used. Unlike with a biplane system which can acquire two images simultaneously, the monoplane system must acquire the two fluoroscopic image sequences sequentially. This requires two contrast injections and two image acquisitions. The standard clinical C-arm angulations for a CRT procedure are anterior-posterior (AP) 0°, left anterior oblique (LAO) 30° and right anterior oblique (RAO) 30°. The proposed method can use any combination of these angulations. To estimate the correct heart phase in the two acquisitions, electrocardiogram-based

(ECG) or an image-based motion gating can be performed. It is proposed to use an image-based motion gating approach that does not rely on ECG data, to have a more generically applicable method. The end diastolic frame of each sequence is selected by an approach based on masked principle component analysis [16]. The method extracts cardiac motion by band pass filtering the variation of the first principle component. Furthermore, it is verified that the selected frames have a sufficient contrast agent fill for segmentation.

2.3.2. 2D vessel detection

The vessels in the contrasted X-ray sequences are segmented and skeletonized to extract the centerline of the CS and its tributary coronary veins. The proposed approach is agnostic to the segmentation method, it can work with automatic, semi-automatic or manual. Automatic [17] and semi-automatic approaches [18] exist for coronary vessel segmentation. In the developed framework a semi-automatic segmentation is performed. This is consistent with other registration approaches for CRT interventions [8, 9]. An average intensity image is computed from all frames of the venogram sequence. The frame to be segmented is divided by the average image, to eliminate static structures, e.g. the spine and static instruments. The resulting image is filtered with a median filter. The Frangi vesselness filter is applied to the smooth image to enhance vascular structures [19]. The vesselness map is binarized by a manually set threshold, such that only strong response is shown. The resulting mask is manually adjusted if necessary: misclassifications are removed, such as instruments and tubular non-vascular structures. The resulting segmentation is skeletonized [20] to create a binary mask of the centerline of the vessels. In order to efficiently and accurately process the 3D reconstruction, the binary centerline is approximated by polylines by the Ramer-Douglas-Peucker algorithm [21, 22], see Figure 3.

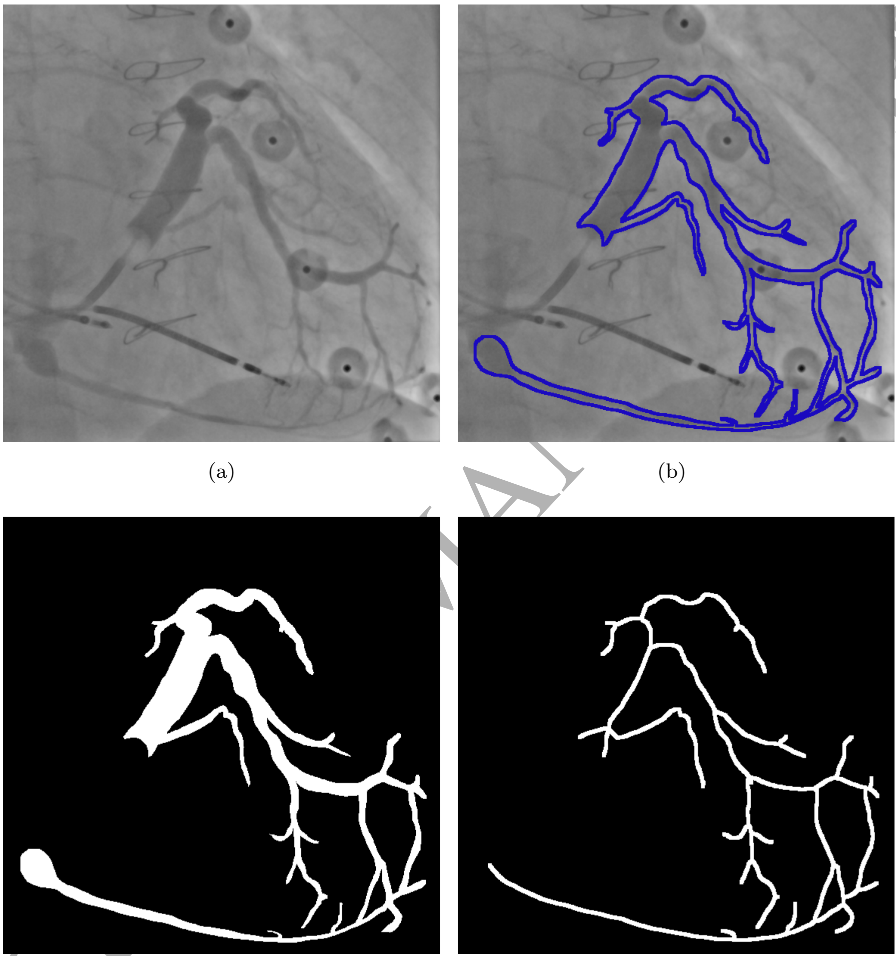

(a)

(b)

(c)

(d)

Figure 3: Vessel segmentation from contrasted X-ray images. (a) Initial contrasted X-ray frame. (b) Semi-automatic segmentation of coronary veins overlayed onto the frame. (c) Binarized segmentation image. (d) Extracted vessel centerlines represented by polylines.

2.3.3. Automatic superabundant 3D vessel reconstruction

The extracted 2D vessels can be reconstructed in 3D if the vessel correspondence and C-arm geometry (epipolar constraint) are known. However, in CRT it is challenging to automatically detect the correct correspondences; the capture of fluoroscopy images at different angulations causes that the vessels have different visual appearance, the images are acquired with two separate manual contrast injections that may not be consistent, contrast can be poor if the balloon is not fully deployed, parts of the vessel system can be self-occluding or out of the field of view of one of the images and the vessel structure can be complex causing multiple potential correspondences. Furthermore, small phase matching errors of an image pair might result in large reconstruction errors if a wrong correspondence is selected, thus could greatly diminish registration accuracy.

To address the challenges outlined above, this paper proposes a fundamentally different approach to 3D reconstruction of the vessels. Instead of establishing one-to-one vessel correspondence and generating a high quality 3D model, the proposed approach uses multiple correspondences and reconstructs a superabundant 3D model. The benefit of this approach is that the reconstructed superabundant 3D model is guaranteed to contain the actual vessel structure, although it will also contain a significant amount of incorrect data or outliers.

The process of reconstructing a superabundant 3D vessel model is shown in Figure 4. The polyline representing the vessel structure in the first fluoroscopic image is traversed, sampling at every 25 pixels. Since the projection geometry of the C-arm acquisition system is known (extracted from the system), epipolar lines of each point can be projected into the second image. All intersections between the epipolar line and the polyline in the second image are computed to generate multiple correspondences. Using the polylines in the second image instead of the centerline mask gives sub pixel intersection accuracy. The points are triangulated to reconstruct the 3D vessel model. The structure of the resulting superabundant 3D vessel model is not noisy or unordered data. It has a vascular, tree like structure where some of the reconstructed branches are

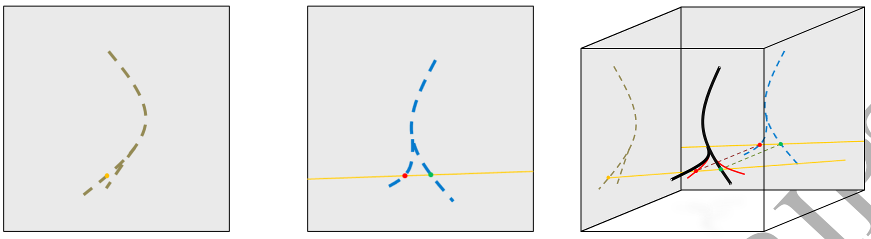

(a) (b) (c)

Figure 4: Reconstruction of a vessel from two views. (a) View one with point to reconstruct (yellow). (b) View two with cast epipolar line (yellow), correct (green) and false correspondence (red). (c) Reconstruction of vessels from image pair, showing correctly (black) and incorrectly (red) reconstructed vessels.

correct reconstructions and others are erroneous as shown in Figure 4 (c). This reflects the structure of the vessels in the 2D images.

A ratio of correctly reconstructed points in the superabundant point cloud can be defined. The number of CL points to reconstruct from the first view is known. It is assumed that every point in the first image has exactly one correct correspondence. The inlier ratio can be computed by dividing the number of points in the first image by the number of all epipolar correspondences in the second image:

$$\varrho_{in} = \frac{\#\text{points in 1st image}}{\#\text{correspondences in 2nd image}}. \tag{1}$$

It should be noted, even if the two sequences are gated successfully and the two frames are perfectly matched, the vasculature might be deformed differently in different cardiac cycles. This deformation can result in slight inaccuracies in the 3D reconstruction of vascular centerline points that can also affect registration accuracy.

2.4. Registering adjacent anatomy

Multimodal image alignment by registering adjacent anatomy is a novel solution to the problem of having few or no cross-modality landmarks. In CRT, the goal is to register the LV epicardium to the coronary veins. This has two significant challenges. 1) the coronary vessels cover only a small fraction of the surface of the LV, i.e., it is a partial surface registration problem. Approaches to solve problems of this type are susceptible to falling into local minima. 2) The automatically reconstructed 3D veonous model (section 2.3.3) contains a large number of outliers. Individually, these problems can be difficult to solve. Together, they pose a substantial challenge. The proposed approach customizes and extends the globally optimal ICP (Go-ICP) algorithm [13, 14], making it robust to large number of outliers by dynamically setting the trimming factor.

2.4.1. Globally optimal registration for partial surfaces

The standard formulation of the registration problem is

$$E(\mathbf{R}, \mathbf{t}) = \sum_{i=1}^{N} e_i^2(\mathbf{R}, \mathbf{t}) = \sum_{i=1}^{N} ||\mathbf{R}\mathbf{x}_i + \mathbf{t} - \mathbf{y}_{j^*}||^2, \tag{2}$$

where $\mathbf{x}$ represents the vessel point cloud, $\mathbf{y}$ the epicardial points, e_i is the error of point i depending on the rotation $\mathbf{R}$ and the translation $\mathbf{t}$, N represents the number of data points and $\mathbf{y}_{j^*}$ the optimal correspondences.

The iterative closest points (ICP) algorithm [23] and its variants can be applied to solve this, however, it suffers from finding local minima and not the global optimum. Alternatively, the branch and bound (BnB) algorithm finds the global optimum, but requires the whole search space to be processed making it computationally expensive [24, 25]. It has been shown that by combining these two methods the global optimum can be found with reduced computational complexity [13, 14].

This approach is an encapsulation of two BnB algorithms and ICP to accelerate the optimization. The outer BnB algorithm operates on the rotation space SO(3), parameterized by the cube $[-\pi, \pi]^3$ and the inner one on the translation space $\mathbb{R}^3$, parametrized by $[-\xi, \xi]^3$, where π and ξ are the half side lengths of the initial cubes respectively. The lower bound for BnB is defined by

$$\underline{E} \doteq \sum_{i=1}^{N} \underline{e}_i^2 = \sum_{i=1}^{N} \max(e_i(\mathbf{R}_{\mathbf{r}_0}, \mathbf{t}_0) - \gamma, 0)^2, \tag{3}$$

where (r_0, t_0) represents the center of the current subspace $C_r \times C_t$ defined by the subcubes for rotation and translation respectively, $\gamma = \gamma_t + \gamma_r$ is the total uncertainty radius, that consists of the maximal distance in the current subcube from the center for the translation and the rotation respectively.

The algorithm subdivides the initial cube into octants (into eight subspaces), see Figure 5, and processes the subcubes in an order from the smallest lower bound to the highest. The upper bound is defined by

$$\overline{E} \doteq \sum_{i=1}^{N} \overline{e}_i^2 = \sum_{i=1}^{N} e_i^2(\mathbf{R}_{\mathbf{r}_0}, \mathbf{t}_0), \tag{4}$$

that is equivalent to the point mathing error at the center of the current subspace (r_0, t_0). If the upper bound $\overline{E}$ is below the current best estimate E^*, ICP is called. If the current best error estimate E^* and the lower error bound $\underline{E}$ are within a preset threshold ϵ, $E^* - \underline{E} < \epsilon$, the optimal solution is found.

The LV and CS models are centered and scaled to be in the interval $[-1, 1]$. Thus the range of translation can be limited to $[-1, 1]$. The orientation was limited to be in the range of $[-35°, 35°]$ which captures the clinically feasible range of rotations.

2.4.2. Dynamic outlier trimming factor

To cope with outliers resulting from the superabundant vessel reconstruction, the Go-ICP variant with trimming was used [14]. The trimmed Go-ICP algorithm amends the error bounds to use only a fraction of the vessel points for the current registration step and uses the trimmed ICP algorithm [26]. The fraction of points to exclude is called trim fraction and can be estimated by calculating the inlier ratio as described in section 2.3.3 and inverting: $\rho_{\text{trim}} = 1 - \rho_{\text{in}}$.

The new lower bound is defined by the subset of points that are closest to

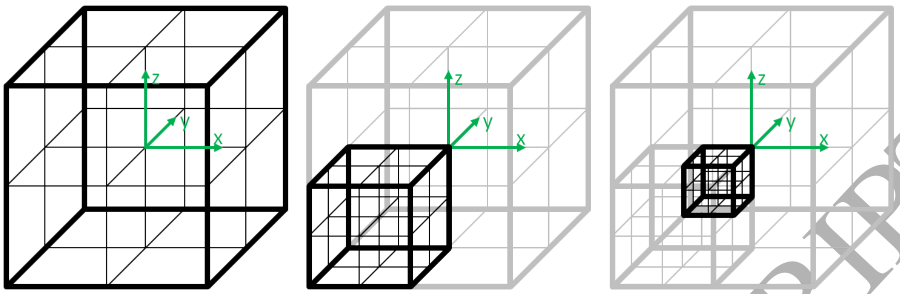

(a) (b) (c)

Figure 5: Go-ICP search space subdivision at the example of translation (same is valid for rotation). (a) Whole search space is subdivided into eight subcubes. (b) Most promising subcube is investigated and subdivided. (c) Subdivision is performed recursively for previous subcube.

the other point cloud in the current iteration as

$$\underline{E} \doteq \sum_{i=1}^{Q} \underline{e}_i^2, \tag{5}$$

where Q is the number of points in the closest subset defined by ρ_{trim}. And the upper bound is defined by

$$\overline{E} \doteq \sum_{i=1}^{Q} \overline{e}_i^2. \tag{6}$$

2.5. Imaging parameters

The MR images are part of a standard cardiac protocol, non contrast-enhanced SA and LA steady state free precession (SSFP) cine images with a flip angle of 52°, on a Siemens Aera 1.5 T MR scanner. The SA stack has a resolution of 192 rows by 156 columns with a pixel spacing of 1.5625 mm and a slice thickness of 8 mm with a gap of 2 mm between slices. The LA image was either a two, a three or a four chamber image. The LA image was acquired with a resolution of 156 rows by 192 columns with the same pixel spacing as the SA slices and a slice thickness of 6 mm. Both sequences were acquired over one cardiac cycle with 25 phases.

The X-ray images were acquired with a Siemens Artis interventional C-arm X-ray system. The images are sequences with 7.5 frames/s and the imaging detector has a resolution of 1920×2048 pixels with a pixel spacing of 0.154 mm. The acquisitions are performed with different magnification factors and collimation. The sequences are acquired with a retrograde manual contrast agent injection with balloon occlusion to highlight the CS and its branching veins.

3. Results

The presented method was evaluated on a phantom dataset, a clinical patient computed tomography angiography (CTA) dataset where a ground truth registration is available and on nine clinical CRT cases. The experiments were performed for all datasets with known correspondence-based and superabundant vessel reconstructions.

3.1. Experiments

To evaluate the performance of the registration method, the same experiments were performed for the phantom and the clinical CTA dataset. The experiments were performed for both, the known corresponcence-based and the superabundant, vessel reconstructions. The ground truth mesh was repeatedly perturbed by a rotation around a specific coordinate axis (x, y or z). The rotation is in the range of -30 to $30°$ with $10°$ steps. No translation was applied, since the point clouds are centered as a first step of the registration as described in section 2.4.1. Next, the disturbed mesh was registered to the respective reconstructed vessel point cloud with the Go-ICP method, with the iterative closest point (ICP) [23] and coherent point drift (CPD) [27] methods for comparison. Finally, the vertex-to-vertex mean absolute error (MAE) was measured.

3.2. Phantom data

To be able to evaluate the performance of our method in a controlled environment with ideal data, a specially designed phantom was created. The epicardial shell of the LV of a CRT patient was segmented from a 3D whole heart MR dataset. The shell was 3D printed and metal wires were attached to model coronary veins. The model was imaged with the clinical C-arm X-ray system. A 3D dataset was acquired by a cone beam CT (CBCT) acquisition. X-ray images at multiple angulations were recorded in the exact same pose. Finally, the acquired CBCT volume was manually segmented and a 3D surface model of the epicardium was extracted. The same pose guarantees that the X-ray images and the segmented epicardial model are in the same coordinate system, see Figure 6.

It is however to be noted that the registration is still not error-free. The residual error consists of segmentation inaccuracies and errors resulting from the 3D model generation from the segmentation. Small registration errors can occure due to calibration inaccuracies of the CBCT reconstruction. To minimize the effect of calibration inaccuracies, the X-ray system was calibrated by a Siemens engineer. The slight errors of the ground truth registration are visible in Figure 6.

With the phantom dataset acquired, two experiments were performed. A registration experiment with known vessel correspondences, to prove that a registration is possible with the available data and a second experiment, with all epipolar correspondences reconstructed, thus with superabundant reconstruction.

3.2.1. Registration with known vessel correspondences

To evaluate the method under ideal circumstances, an experiment was performed with a vessel reconstruction of known point correspondences. First two images were selected having an angular difference of 60 degrees, that is typical for cardiac (especially CRT) interventions, see Figure 6. Since the attached wires that represent the vessels are well contrasted, they can be easily separated from the background by simple thresholding. The thresholded binary images are skeletonized to extract the centerlines of the wires, as described in section 2.3.2. The components of the centerlines are subdivided into separate images, such that only one centerline (or a section of a centerline) with known correspondece

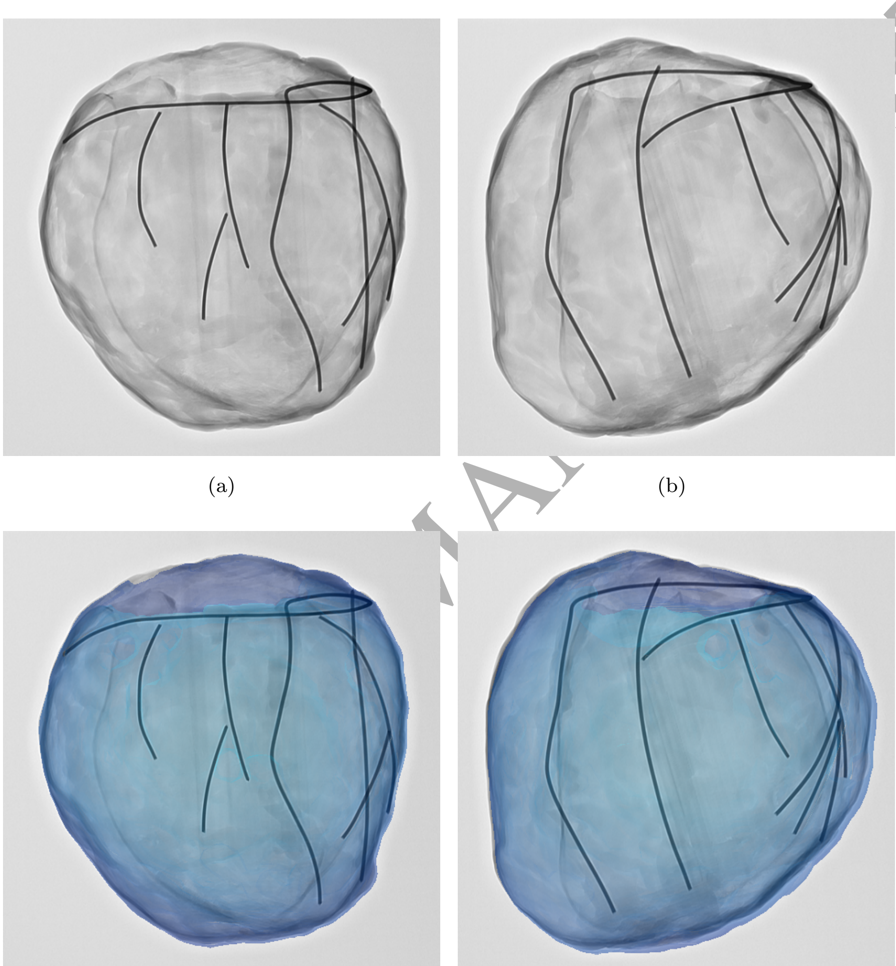

(a) (b) (c) (d)

Figure 6: Created phantom dataset. (a, b) LAO 30° and RAO 30° X-ray acquisitions of the phantom. (c, d) Epicardial mesh, segmented from MRI, overlayed onto the two X-ray images.

can stay in an image pair. This guarantees that for each point in image one there is only one corresponding point in image two, thus resulting in an ideal, outlier-free reconstruction.

The repeated rotation experiment (section 3.1) with known correspondences shows, that the Go-ICP registration outperforms the other point cloud registration methods, see Figure 7 (a-c). ICP might even fail if the rotation is small, the initial alignment is close to the optimal solution. ICP registration resulted in an average MAE of 9.54±5.6 mm. CPD is more robust against rotation, often finds the optimal rotation for higher angles too. The CPD algorithm resulted in an average MAE of 4.9±4.03 mm. The average MAE of Go-ICP was 2.68±0.17 mm. This small error can be explained by the previously in section 3.2 mentioned error factors.

3.2.2. Superabundant point cloud registration

To simulate a scenario that could be applied to a clinical dataset, the registration experiment with the superabundant vessel reconstruction was performed, as described in section 2.3.3.

Since the outliers disturb and prevent an accurate registration, Go-ICP with trimming was used. The trim fraction ρ_{trim} was determined by the vessel point cloud reconstruction as described in section 2.4.2. The estimated trim fraction for the phantom dataset was 0.79. An experiment was performed where the trim fraction was varied and the resulting error of the automatically registered mesh was measured, see Figure 8. The experiment has shown that the error is minimal in the range of 0.80 to 0.85, thus comparable with the estimated value.

The rotation experiment was performed and the registration results were compared to the ones of the registration with known vessel correspondences. The registration results in slightly worse mean errors for the superabundant reconstruction, the average MAE is 3.87 ± 1.22 mm, the Go-ICP method clearly outperforms ICP (average MAE of 32.63 ± 9.52 mm) and CPD (average MAE of 13.26 ± 6.93 mm). ICP fails even if the initial alignment is close to the global optimum. CPD performs well close to the optimum, but its performance

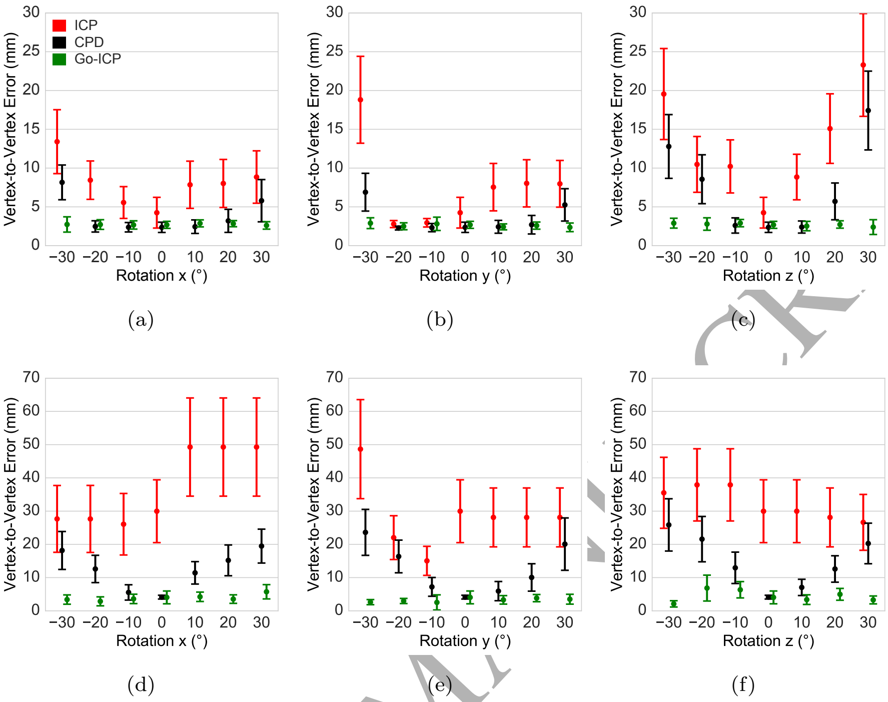

Figure 7: Mean vertex-to-vertex errors and standard deviations of the registered phantom epicardial mesh with the ICP (red), CPD (black) and the Go-ICP (green) methods. (a-c) Errors of registration based on known vessel correspondences. (d-f) Errors of registration based on superabundant reconstruction. Note the difference in the error axis scales.

decreases rapidly for higher rotations, see Figure 7 (d-f).

3.3. Clinical data

After a successfull evaluation on phantom data, the registration method was evaluated on clinical data. First a cardiac CTA dataset was used, since then
350 a ground truth registration is initially available, thus it is possible to prove that the method is capable of registering ideal, but real clinical patient data. Additionally, the method was evaluated qualitatively on nine clinical CRT cases, on one of them quantitatively.

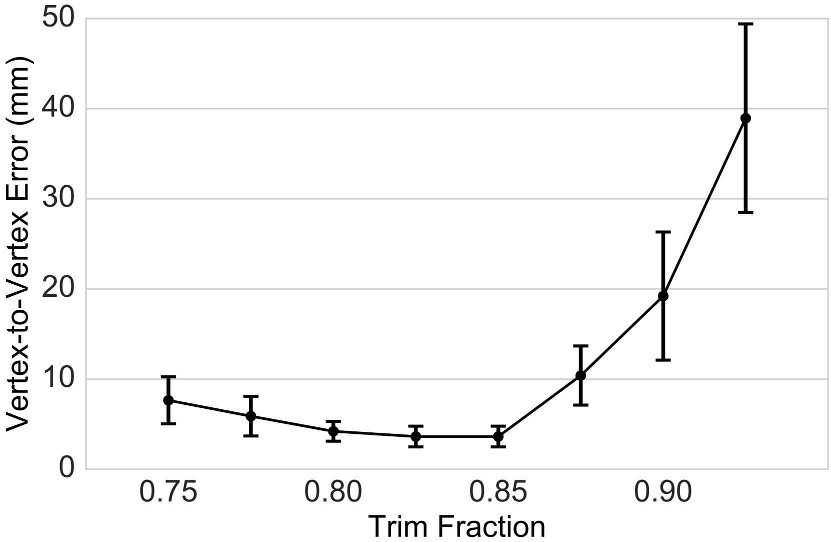

Figure 8: Error over trim fraction of the Go-ICP algorithm for the phantom dataset. For a rotation of 20° around the x axis.

3.3.1. Clinical CTA dataset

The evaluation of the method on clinical data is extremely challenging. Due to the lack of shared landmarks in the two modalities, an accurate ground truth registration is hard to obtain and a target registration error is hard to define. An accurate manual registration by a clinical expert is not feasible, since the registration with six degrees of freedom cannot be easily performed with only two (non-orthogonal) X-ray projections.

To have a clinical dataset where a ground truth registration is available, a CTA dataset was segmented. Since both the vessels and the LV are extracted from the same image data, see Figure 9, both are initially registered, thus a ground truth registration is available and a vertex-to-vertex registration error can be calculated. The CTA segmentation has also revealed, what was also described in the literature [28, 29], that the whole CS does not always lie on the surface of the left ventricle, see Figure 9 (b). For this reason, the root of the CS was removed from the clinical vessel point clouds, since they might disturb

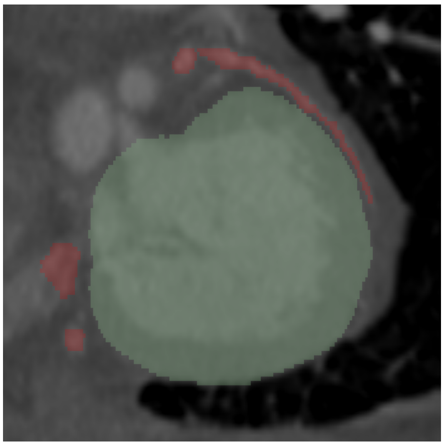

(a)

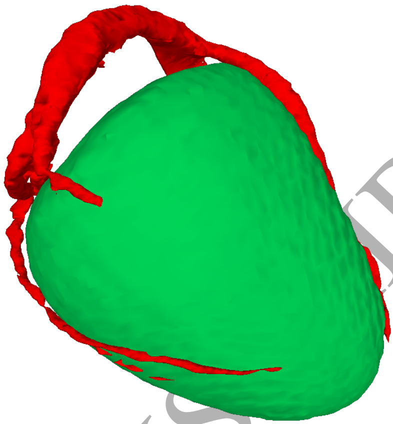

(b)

Figure 9: Segmented CTA dataset. (a) LV epicardial mesh (green) with coronary vein mesh (red). (b) LV epicardial mesh with the coronary vein mesh.

the registration.

The same rotation experiment was performed for the clinical CTA dataset as for the phantom data, as described in section 3.1. The Go-ICP method had an average MAE of 3.65 $\pm$ 0.59 mm, thus has clearly outperformed ICP (6.69 $\pm$ 2.49 mm) and showed also slightly better results than CPD (4.72 $\pm$ 2.1 mm), see Figure 10 (a-c).

In a second experiment, to simulate a dataset with a superabundant vessel reconstruction, points of a uniform random distribution were added in the bounding box of the vessel centerline. The resulting superabundant point cloud had twice as many points as the initial point cloud, thus the trim fraction $\rho_{\text{trim}} = 0.5$. Repeating the same experiment of rotations, Go-ICP could successfully register the epicardial mesh every time to the vessel point cloud, resulting in slightly worse results than in the case of the outlier-free, known correspondence-based point cloud, with an average MAE of 4.24$\pm$0.65 mm. ICP failed in every case with an average error of 20.31$\pm$1.24 mm. CPD could also not find the optimal alignment resulting in an average MAE of 11.56$\pm$2.51 mm. For detailed results,

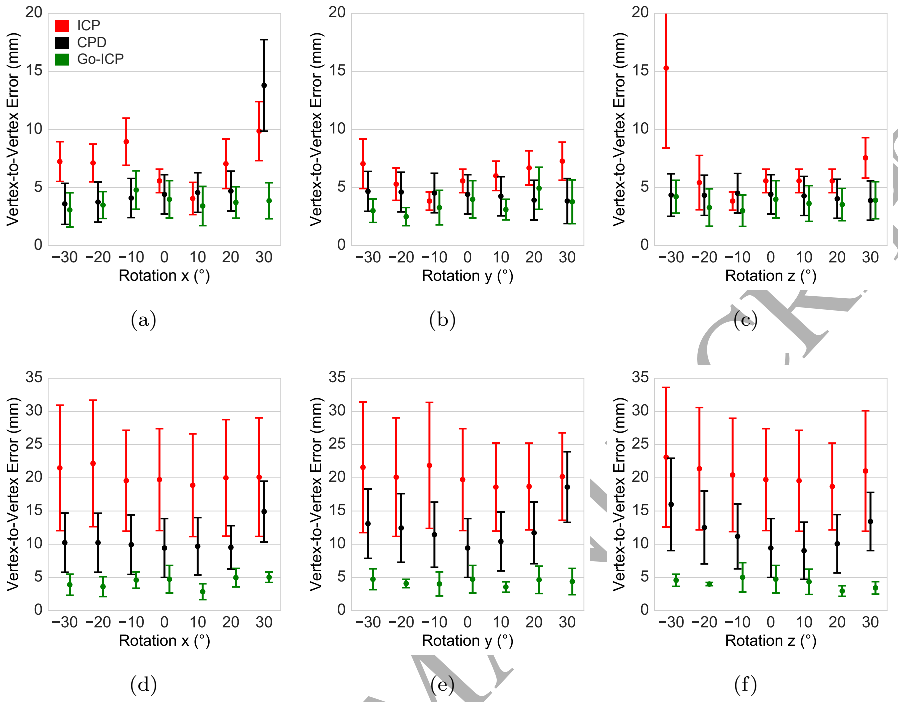

Figure 10: Mean vertex-to-vertex errors and standard deviations of the registered CTA epicardial mesh with the ICP (red), CPD (black) and the Go-ICP (green) methods. (a-c) Errors of registration for the reconstructed vessel CLs. (d-f) Errors of registration for the CLs with added outliers. Note the difference in the error axis scales.

see Figure 10 (d-f).

3.3.2. Clinical CRT datasets

To be able to define an error measure for a real clinical CRT dataset, a novel way to evaluate, using previously implanted artificial valves was developed. Among the available retrospective clinical datasets, one patient had previously implanted artificial aortic and mitral valves that are visible in both modalities, see Figure 11. The valves were segmented in the MRI dataset and their centerpoints were extracted in 3D. The two centerpoints were also reconstructed in 3D from the X-ray acquisitions. Thus, the extracted valve points can be used as multimodality landmarks. The valve points are ideal landmarks to have an estimation of the registration error, since they are located directly at the base of the LV. Additionally, their arrangement defines the rotation of the LV around its long axis.

For the clinical CRT dataset, first, the registration with known vessel correspondences was performed. The results are visually appealing, see Figure 12 (a,b), the overlay shows a good alignment with the shadow of the heart, the coronary veins appear to be on the ventricle and the location of the MRI derived valve centerpoints are close to the centerpoints is the X-ray images. The comparison of the valves in 3D resulted in valve errors of 4.29 mm and 9.13 mm for the aortic and the mitral valves respectively. Considering the resolution of the MR images used for the LV epicardium's segmentation, 1.5625 mm $\times$ 1.5625 mm in plane and 8 mm slice thickness with 2 mm gap between slices, the results are in the range of the slice spacing (slice thickness + gap = 10 mm).

To assess the accuracy of the results, clinical experts were consulted. The experts set the clinical requirement based on the 16 segment model, defined by the American Heart Association (AHA). The clinical team determined that the registration is sufficiently accurate, if the error does not significantly impact the target segment on the LV epicardium. The required accuracy was explicitly defined by the clinical team to be below half of the AHA segment size. The average segment size was found to be 43.4 mm (along short axis) $\times$ 32.7 mm (along long axis). Thus the minimum average half-segment size is 16.35 mm. The resulting valve registration errors satisfy this requirement, being below the average half-segment size.

In the second experiment, the epicardial mesh was registered to the superabundant point cloud. The trim fraction was calculated to be 0.44, thus $\rho_{\mathrm{trim}} = 0.44$ was used in the registration. The results are visually comparable with the results of the registration with known vessel correspondences, see Figure 12. This was also proven by the 3D valve errors. The aortic valve error was 2.94 mm and the mitral valve error was 3.86 mm, thus the errors differ only slightly from the known correspondence-based reconstruction's, the difference is in the range of the MR resolution.

The registration results are sufficiently accurate for the clinical use case of CRT (below the clinical requirement of 16.35 mm), however the registration error could be further reduced. The accuracy of the system is affected by MR resolution and to a lesser extent MR segmentation and vessel reconstruction. The main limitation of accuracy is the very low out of plane resolution (10 mm) and low in plane resolution (1.5625 mm) of the MR images compared with CT which can have submillimetre voxels. Furthermore, this low resolution can introduce inaccuracies in the MR segmentation of the LV and manual annotation of the valves used for evaluation. Additional small sources of error can come from the segmentation and skeletonization of the vessels in X-ray and small inaccuracies in the phase gating between the two X-ray images which is limited by the frame rate (7.5 fps). Inaccuracies in these steps can lead to 3D vessel reconstruction error, however this was not observed to be significant.

To further improve the accuracy of the system, future work will explore the use of experimental high resolution MR protocols. Such protocols are not currently a clinical standard due to the long acquisition time and breath hold requirement, however, this is an active research area with promising initial results.

The registration with superabundant vessel reconstruction was evaluated on eight further CRT patients. Since no landmarks, such as artificial valves, were available, the registration was evaluated qualitatively by eightclinical experts, by visual inspection and scoring. The clinical experts assigned the overlay pairs of each patient to one of the four categories: 3. no correction is necessary for interventional guidance, 2. minor corrections are necessary, 1. major corrections are necessary and 0. registration has failed, alignment is not useful for interventional guidance. This resulted in 72 cases in total (8 experts $\times$ 9 patients). Scores of 3 or 2 were given in 95.8 % of cases, i.e., no, or only minor correction is necessary. Only 4.2 % of cases were rated with 1, requiring major correction. No failure was identified. The average rating of the registration was 2.31 ± 0.27. For a detailed summary of the results see Table 1.

The mean runtime for the nine CRT patients was 95.24 s on an Intel Core i7 with 8GB RAM. The preprocessing time of the X-ray images and the runtime of the algorithm is acceptable for CRT procedures, since after the contrast agent injection was performed, the clinical team has to prepare for the LV lead implant. The occlusion balloon has to be removed, the catheter delivering the lead has to be prepared and inserted into the coronary sinus. It should be noted that the current implementation is single-threaded. A multi-threaded implementation could explore the search space in parallel, thus could greatly reduce runtime.

The overlay pairs for three patients are shown in Figure 13. The results are visually appealing, the projected epicardial model's border corresponds well to the heart shadow, except for minor discrepancies and the coronary veins appear mainly on the left ventricle in the images. Figure 13 (e-f) show that the registration results in good visual alignment even for extensively cropped X-ray images.

It should also be noted that the registration appears to be robust against that the two images are not acquired simulteaneously with a biplane system. Since the images are acquired with the same plane rotated, even after the frame matching was performed, as described in section 2.3.1, the vasculature might have deformed between the acquisitions. These slight deformations can affect the reconstruction accuracy, but the results indicate the robustness of the method against them.

4. Conclusion

This paper has presented a novel approach of registration for cardiac interventions and a novel approach for evaluation by using implanted artificial valves. The idea is to use adjacent anatomical structures, the left ventricle segmented from cardiac MR images and a point cloud of the cornary veins that was reconstructed from two interventional X-ray images without knowing point correspondences, resulting in a superabundant point cloud. The reconstructed vessel point cloud has a high ratio of outliers, since all epipolar correspondences

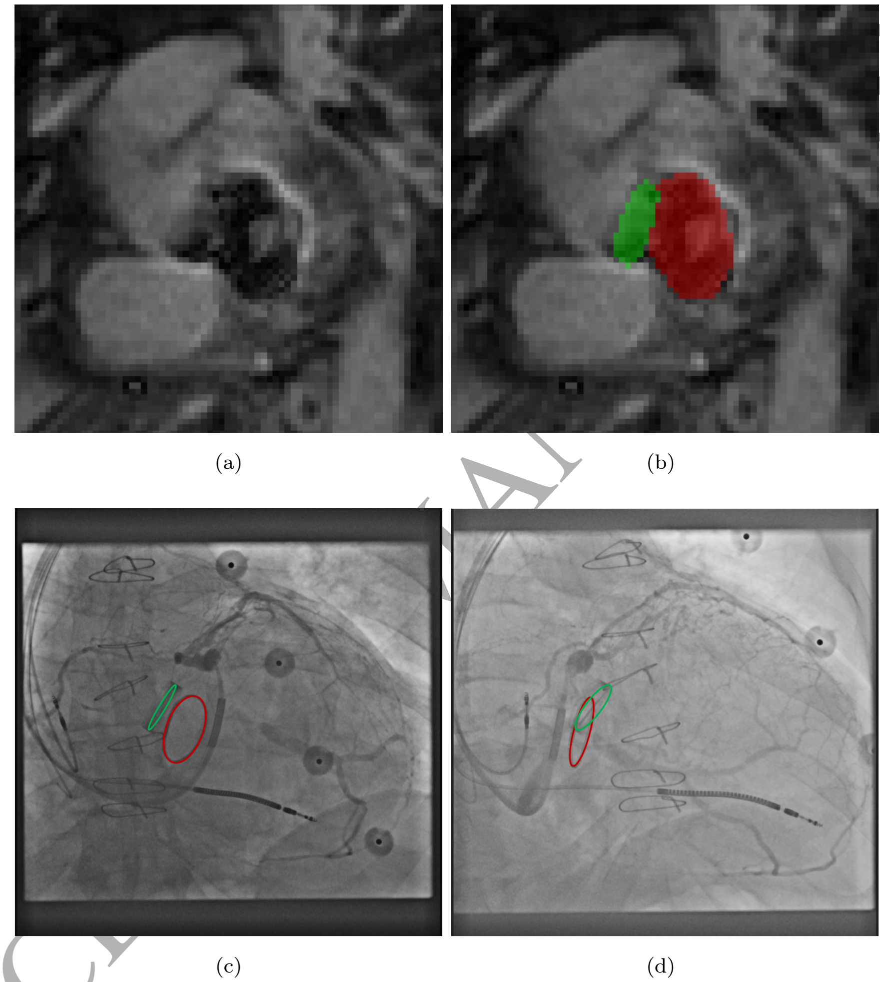

Figure 11: Artificial valve extraction. (a) MR slice showing artificial aortic and mitral valves. (b) MR slice showing segmented aortic (green) and mitral (red) valves. (c) LAO 1.4° X-ray view. (d) RAO 31.3° X-ray image.

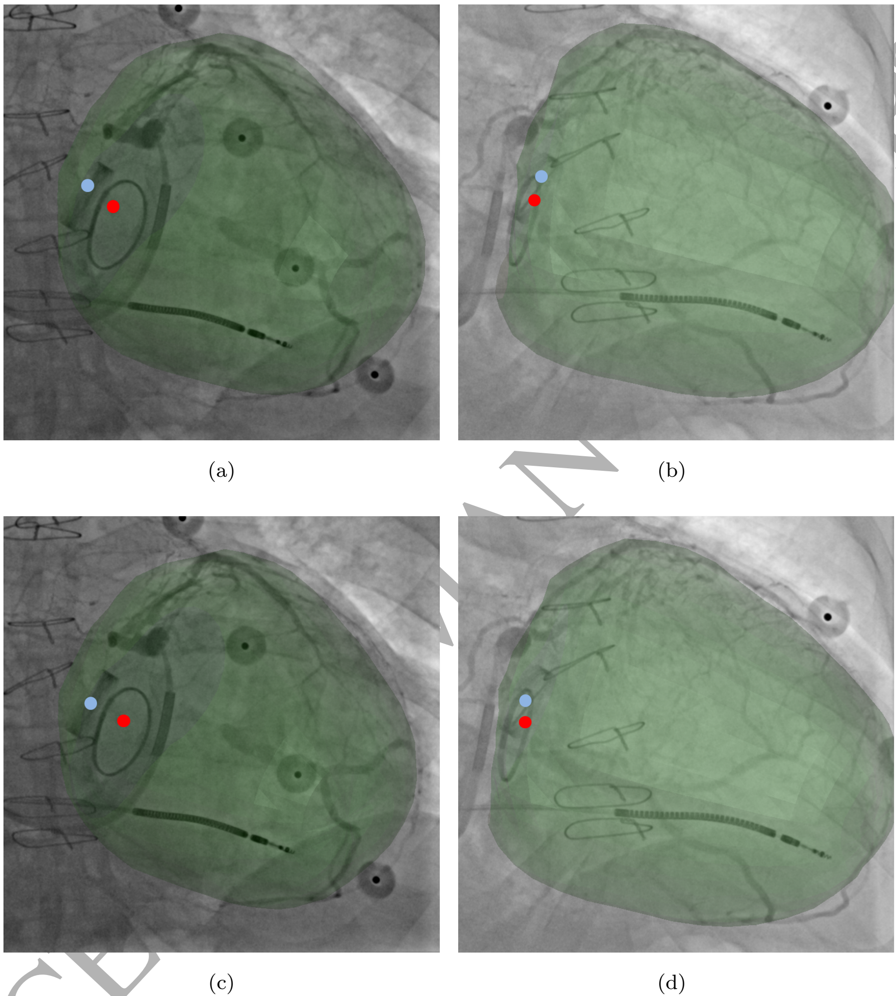

Figure 12: Registered epicadial mesh (green), aortic valve centroid (blue) and mitral valve centroid (red) overlayed. (a) LAO 1.4° X-ray view of registration with known vessel corrrespondences. (b) RAO 31.3° X-ray view of registration with known vessel corrrespondences. (c) LAO 1.4° X-ray view of registration with superabundant vessel point cloud. (d) RAO 31.3° X-ray view of registration with superabundant vessel point cloud.

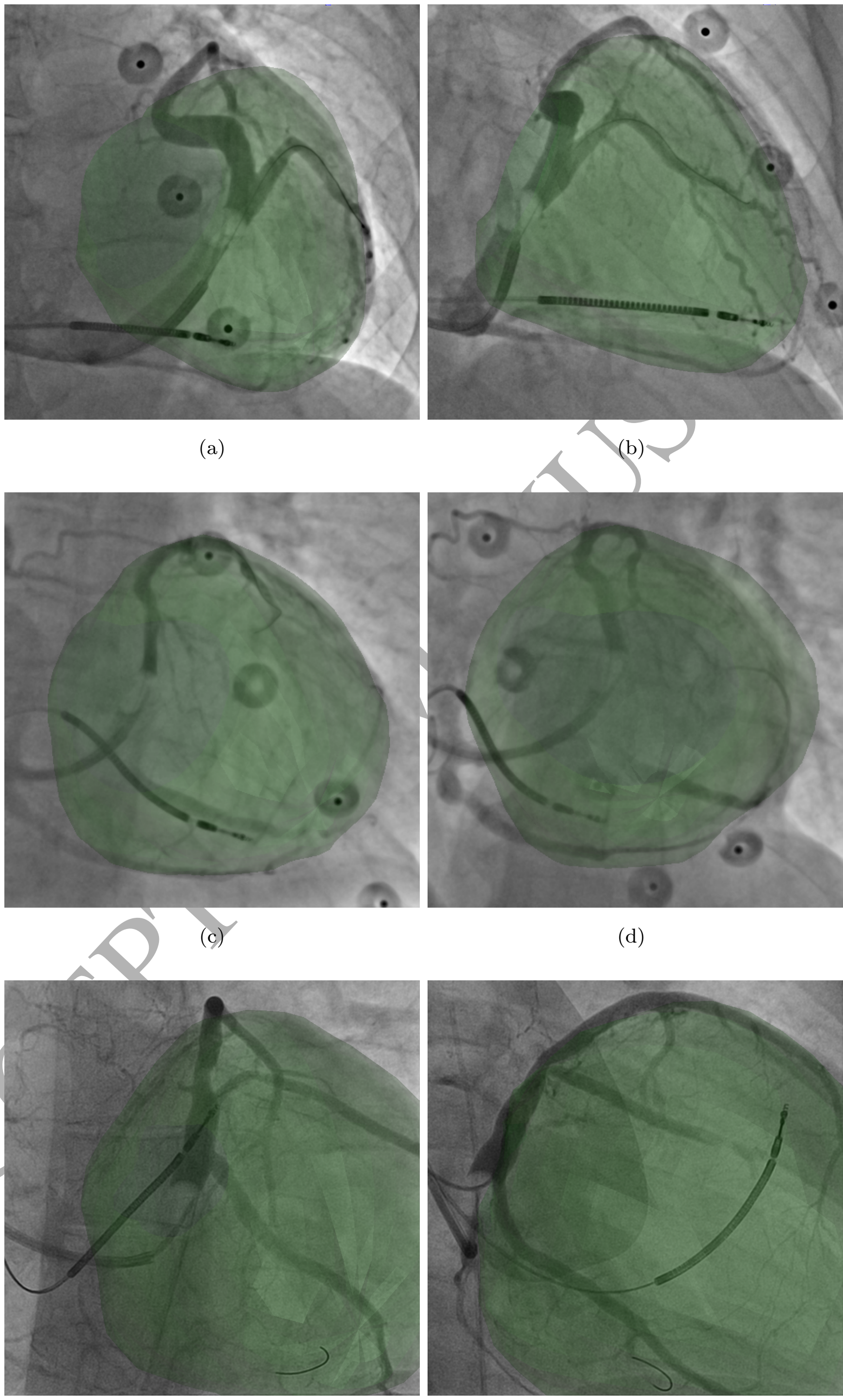

(e) (f)

Figure 13: Overlay of registered epicardial shell for three CRT patients. (a) Patient 1 – AP (LAO-RAO 0°) view. (b) Patient 1 – RAO 30° view. (c) Patient 3 – LAO 1° view. (d) Patient 3 – LAO 29° view. (e) Patient 5 – LAO 18° view. (f) Patient 5 – RAO 30° view.

Table 1: Qualitative assessment of registration results by eightclinical experts for 9 CRT patients. Scores: 3. no correction is necessary for interventional guidance, 2. minor corrections are necessary, 1. major corrections are necessary and 0. registration has failed.

	Patients								
	P1	**P2**	**P3**	**P4**	**P5**	**P6**	**P7**	**P8**	**P9**
Expert 1	2	3	3	2	2	3	2	2	2
Expert 2	2	3	3	2	2	2	2	2	2
Expert 3	2	3	2	3	3	3	2	2	2
Expert 4	2	3	3	2	3	3	2	2	2
Expert 5	3	2	1	2	2	2	2	2	2
Expert 6	2	2	2	2	3	2	2	1	2
Expert 7	2	3	2	2	3	3	3	3	2
Expert 8	3	3	2	1	2	3	3	3	2
Mean	2.3	2.8	2.3	2.0	2.5	2.6	2.3	2.1	2.0
Std. Dev.	0.5	0.5	0.7	0.5	0.5	0.5	0.5	0.6	0.0

were reconstructed. For the registration of the epicardial and the vessel point cloud the Go-ICP algorithm with trimming for outlier rejection was used and the trim fraction was defined dynamically. Experiments on a specially designed phantom have shown, that the method is capable of registering the two point clouds with an average MAE of 3.87 ± 1.22 mm that is superior to other point cloud registration methods, such as ICP and CPD.

Further experiments on a clinical CTA dataset have shown, that the registration method is able to register clinical data. The average MAE between the ground truth and the registered epicardium was 4.24 ± 0.65 mm, slightly worse than for the phantom dataset.

In a final experiment the method was validated retrospectively on nine clinical CRT cases. The registration results were scored by eightclinical experts on a scale of 0 (worst) to 3 (best). The average score was 2.31 ± 0.27. One of the patients had previously implanted aortic and mitral valves that were segmented from the MR and X-ray images and reconstructed in 3D to define a registration error. After the registration the valve centroids showed relatively low errors in 3D, the 3D aortic valve error was 2.94 mm and the mitral valve error was 3.86 mm. That is in the range of the MR slice spacing of 10 mm. The valve errors are below the clinical requirement defined by the half-segment size of a 16 segment AHA model, found to be 16.35 mm on average. The resulting valve errors suggest that the registration is capable of providing a registration that can be applied for image guidance of cardiac interventions, such as CRT delivery.

Acknowledgements and disclaimer

The authors are grateful for the support from the Innovate UK grant 32684-234174. The research was supported by the National Institute for Health Research (NIHR) Biomedical Research Centre based at Guy's and St Thomas' NHS Foundation Trust and King's College London. The views expressed are those of the author(s) and not necessarily those of the NHS, the NIHR or the Department of Health. This study complied with the Declaration of Helsinki and the protocol was approved by the local ethics committee. Informed written consent was obtained from each patient. Concepts and information presented are based on research and are not commercially available.

References

[1] S. Claridge, Z. Chen, T. Jackson, K. De Silva, J. Behar, M. Sohal, J. Webb, E. Hyde, M. Lumley, K. Asrress, R. Williams, J. Bostock, M. Ali, J. Gill, M. O'Neill, R. Razavi, S. Niederer, D. Perera, C. A. Rinaldi, Effects of Epicardial and Endocardial Cardiac Resynchronization Therapy on Coronary Flow: Insights From Wave Intensity Analysis., Journal of the American Heart Association 4 (12) (2015) 1–12. doi:10.1161/JAHA.115.002626.

[2] J.-C. Daubert, L. Saxon, P. B. Adamson, A. Auricchio, R. D. Berger, J. F. Beshai, O. Breithard, M. Brignole, J. Cleland, D. B. DeLurgio, K. Dickstein, D. V. Exner, M. Gold, R. A. Grimm, D. L. Hayes, C. Israel, C. Leclercq, C. Linde, J. Lindenfeld, B. Merkely, L. Mont, F. Murgatroyd, F. Prinzen, S. F. Saba, J. S. Shinbane, J. Singh, A. S. Tang, P. E. Vardas, B. L. Wilkoff, J. L. Zamorano, I. Anand, C. Blomström-Lundqvist, J. P. Boehmer, H. Calkins, S. Cazeau, V. Delgado, N. M. Estes, D. Haines, F. Kusumoto, P. Leyva, F. Ruschitzka, L. W. Stevenson, C. T. Torp-Pedersen, 2012 EHRA / HRS Expert Consensus Statement on Cardiac Resynchronization Therapy in Heart Failure: Implant and Follow-up Recommendations and Management, Heart Rhythm 9 (9) (2012) 1524–1576. doi:10.1016/j.hrthm.2012.07.025.

[3] R. de Silva, L. F. Gutiérrez, A. N. Raval, E. R. McVeigh, C. Ozturk, R. J. Lederman, X-Ray Fused with Magnetic Resonance Imaging (XFM) to Target Endomyocardial Injections: Validation in a Swine Model of Myocardial Infarction., Circulation 114 (22) (2006) 2342–2350. doi:10.1161/CIRCULATIONAHA.105.598524.

[4] K. S. Rhode, D. L. G. Hill, P. J. Edwards, J. Hipwell, D. Rueckert, G. Sanchez-Ortiz, S. Hegde, V. Rahunathan, R. Razavi, Registration and Tracking to Integrate X-ray and MR Images in an XMR Facility, IEEE Transactions on Medical Imaging 22 (11) (2003) 1369–1378. doi:10.1109/TMI.2003.819275.

[5] F. Bourier, A. Brost, L. Yatziv, J. Hornegger, N. Strobel, K. Kurzidim, Coronary Sinus Extraction for Multimodality Registration to guide Transseptal Puncture, in: T. Kahn, F. A. Jolesz, J. S. Lewin (Eds.), 8th Interventional MRI Symposium, Leipzig, 2010, pp. 311–313.

[6] M. V. N. Truong, A. Aslam, C. A. Rinaldi, R. Razavi, G. P. Penney, K. S. Rhode, Preliminary Investigation : 2D-3D Registration of MR and X-ray Cardiac Images Using Catheter Constraints, in: MICCAI Workshop on

Cardiovascular Interventional Imaging and Biophysical Modelling, London, 2009, pp. 1–9.

[7] J. Choi, P. Radau, R. Xu, G. A. Wright, X-Ray and Magnetic Resonance Imaging Fusion for Cardiac Resynchronization Therapy, Medical Image Analysis 31 (2016) 98–107. doi:10.1016/j.media.2016.03.004.

[8] T. L. Faber, C. A. Santana, E. V. Garcia, J. Candell-Riera, R. D. Folks, J. W. Peifer, A. Hopper, S. Aguade, J. Angel, J. L. Klein, Three-Dimensional Fusion of Coronary Arteries with Myocardial Perfusion Distributions: Clinical Validation, Journal of Nuclear Medicine 45 (5) (2004) 745–753.

[9] W. Zhou, X. Hou, M. Piccinelli, X. Tang, L. Tang, K. Cao, E. V. Garcia, J. Zou, J. Chen, 3D Fusion of LV Venous Anatomy on Fluoroscopy Venograms With Epicardial Surface on SPECT Myocardial Perfusion Images for Guiding CRT LV Lead Placement, JACC: Cardiovascular Imaging 7 (12) (2014) 1239–1248. doi:10.1016/j.jcmg.2014.09.002.

[10] D. L. G. Hill, D. J. Hawkes, Medical Image Registration Using Knowledge of Adjacency of Anatomical Structures, Image and Vision Computing 12 (3) (1994) 173–178. doi:10.5244/C.7.44.

[11] D. Toth, M. Panayiotou, A. Brost, J. M. Behar, C. A. Rinaldi, K. S. Rhode, P. Mountney, Registration with Adjacent Anatomical Structures for Cardiac Resynchronization Therapy Guidance, in: Statistical Atlases and Computational Models of the Heart, 2016.

[12] A. Iskurt, Y. Becerikli, K. Mahmutyazicioglu, A Fast and Automatic Calibration of the Projectory Images for 3D Reconstruction of the Branchy Structures, in: 47th Annual Conference on Information Sciences and Systems (CISS)., 2013, pp. 1–6.

[13] J. Yang, H. Li, Y. Jia, Go-ICP: Solving 3D Registration Efficiently and

Globally Optimally, in: 2013 IEEE International Conference on Computer Vision, 2013, pp. 1457–1464. doi:10.1109/ICCV.2013.184.

[14] J. Yang, H. Li, D. Campbell, Y. Jia, Go-ICP: A Globally Optimal Solution to 3D ICP Point-Set Registration, IEEE Transactions on Pattern Analysis and Machine Intelligence 38 (11) (2016) 2241–2254. doi:10.1109/TPAMI.2015.2513405.

[15] M.-P. Jolly, C. Guetter, X. Lu, H. Xue, J. Guehring, Automatic Segmentation of the Myocardium in Cine MR Images Using Deformable Registration, in: Statistical Atlases and Computational Models of the Heart - Imaging and Modelling Challenges, Vol. 8896, 2011, pp. 105–113. arXiv:9780201398298, doi:10.1007/978-3-642-28326-0_26.

[16] M. Panayiotou, A. P. King, R. J. Housden, Y. Ma, M. Cooklin, M. O'Neill, J. Gill, C. A. Rinaldi, K. S. Rhode, A Statistical Method for Retrospective Cardiac and Respiratory Motion Gating of Interventional Cardiac X-Ray Images, Medical Physics 41 (7) (2014) 071901. doi:10.1118/1.4881140.

[17] E. Nasr-Esfahani, S. Samavi, N. Karimi, S. Soroushmehr, K. Ward, M. Jafari, B. Felfeliyan, B. Nallamothu, K. Najarian, Vessel extraction in X-ray angiograms using deep learning, in: 38th Annual International Conference of the IEEE Engineering in Medicine and Biology Society (EMBC), 2016, pp. 643–646. doi:10.1109/EMBC.2016.7590784.

[18] S.-Y. Sun, P. Wang, S. Sun, T. Chen, Model-Guided Extraction of Coronary Vessel Structures in 2D X-Ray Angiograms, in: P. Golland, N. Hata, C. Barillot, J. Hornegger, R. Howe (Eds.), Medical Image Computing and Computer-Assisted Intervention – MICCAI 2014, Vol. 8674, Springer, Boston, 2014, pp. 594–602. doi:10.1007/978-3-319-10470-6_74.

[19] A. F. Frangi, W. J. Niessen, K. L. Vincken, M. a. Viergever, Multiscale vessel enhancement filtering, in: Medial Image Computing and Computer-Assisted Invervention - MICCAI'98. Lecture Notes in Computer Science, vol 1496, 1998, pp. 130–137. doi:10.1016/j.media.2004.08.001.

[20] Y. S. Chen, W. H. Hsu, A Modified Fast Parallel Algorithm for Thinning Digital Patterns, Pattern Recognition Letters 7 (2) (1988) 99–106. doi:10.1016/0167-8655(88)90124-9.

[21] U. Ramer, An Iterative Procedure for the Polygonal Approximation of Plane Curves, Computer Graphics and Image Processing 1 (3) (1972) 244–256. doi:10.1016/S0146-664X(72)80017-0.

[22] D. H. Douglas, T. K. Peucker, Algorithms for the Reduction of the Number of Points Required to Represent a Digitized Line or its Caricature, Cartographica: The International Journal for Geographic Information and Geovisualization 10 (2) (1973) 112–122. doi:10.3138/FM57-6770-U75U-7727.

[23] P. Besl, N. McKay, A Method for Registration of 3-D Shapes (1992). doi:10.1109/34.121791.

[24] R. J. Dakin, A Tree-Search Algorithm for Mixed Integer Programming Problems, The Computer Journal 8 (3) (1965) 250–255. doi:10.1093/comjnl/8.3.250.

[25] A. H. Land, A. G. Doig, An Automatic Method for Solving Discrete Programming Problems, Econometrica 28 (3) (1960) 497–520. doi:10.2307/1910129.

[26] D. Chetverikov, D. Stepanov, Robust Euclidean Alignment of 3D Point Sets, Image and Vision Computing 23 (3) (2005) 299–309. doi:10.1016/j.imavis.2004.05.007.

[27] A. Myronenko, X. Song, Point-Set Registration: Coherent Point Drift, Pattern Analysis and Machine Intelligence, IEEE Transactions on 32 (12) (2010) 2262–2275. arXiv:0905.2635, doi:10.1109/TPAMI.2010.46.

[28] J. P. Singh, S. Houser, E. K. Heist, J. N. Ruskin, The Coronary Venous Anatomy: A Segmental Approach to Aid Cardiac Resynchronization Therapy, Journal of the American College of Cardiology 46 (1) (2005) 68–74. doi:10.1016/j.jacc.2005.04.017.

[29] N. R. Van de Veire, J. D. Schuijf, J. De Sutter, D. Devos, G. B. Bleeker, A. de Roos, E. E. van der Wall, M. J. Schalij, J. J. Bax, Multimodality Imaging of Anatomy and Function in Coronary Artery Disease, Journal of American College of Cardiology 48 (9) (2006) 1832–1838. doi:10.1016/j.jacc.2006.07.042.